2011

Langevin dynamics for the transport of flexible biological macromolecules in confined geometries

Michael H. Peters
Virginia Commonwealth University, mpeters@vcu.edu

Peters, M. H. Langevin dynamics for the transport of flexible biological macromolecules in confined geometries. The Journal of Chemical Physics 134, 025105 (2011).

Langevin dynamics for the transport of flexible biological macromolecules in confined geometries

Michael H. Peters[a)]
Department of Chemical and Life Science Engineering, Virginia Commonwealth University, Richmond, Virginia 23284, USA

(Received 19 August 2010; accepted 16 November 2010; published online 14 January 2011)

The transport of flexible biological macromolecules in confined geometries is found in a variety of important biophysical systems including biomolecular movements through pores in cell walls, vesicle walls, and synthetic nanopores for sequencing methods. In this study, we extend our previous analysis of the Fokker–Planck and Langevin dynamics for describing the coupled translational and rotational motions of single structured macromolecules near structured external surfaces or walls [M. H. Peters, J. Chem. Phys. **110**, 528 (1999); **112**, 5488 (2000)] to the problem of many interacting macromolecules in the presence of structured external surfaces representing the confining geometry. Overall macromolecular flexibility is modeled through specified interaction potentials between the structured Brownian subunits (*B*-particles), as already demonstrated for protein and DNA molecules briefly reviewed here. We derive the Fokker–Planck equation using a formal multiple time scale perturbation expansion of the Liouville equation for the entire system, i.e., solvent, macromolecules, and external surface. A configurational–orientational Langevin displacement equation is also obtained for use in Brownian dynamics applications. We demonstrate important effects of the external surface on implicit solvent forces through formal descriptions of the grand friction tensor and equilibrium average force of the solvent on the *B*-particles. The formal analysis provides both transparency of all terms of the Langevin displacement equation as well as a prescription for their determination. As an example, application of the methods developed, the real-time movement of an α-helix protein through a carbon nanotube is simulated. © *2011 American Institute of Physics*. [doi:10.1063/1.3525381]

I. INTRODUCTION

The modeling of flexible biological macromolecules represents a critical problem in the understanding of a variety of cellular processes, including cell signal pathways, enzymatic actions, regulation, transcription, and many others. These cellular processes are often the result of specific, directed changes in macromolecular conformations made possible by their inherent flexibility.

Following polymer kinetic theory approaches, nonrigid structured biological macromolecules have been successfully modeled as flexibly connected rigid subunits based on the particular internal bonding behavior of the system. For example, proteins have been effectively modeled as flexibly connected rigid, Brownian subunits.[1–7] Similarly, DNA and RNA have been modeled as flexibly connected rigid elements based on their internal bonding behavior.[8–14]

In addition to inherent flexibility, many important applications of biological macromolecular dynamics involve the presence of a fixed, external surfaces. For example, both DNA and protein cellular physiological processes involve their movement through pores.[15–17] In addition, recently proposed DNA sequencing devices involve threading the macromolecule through structured nanochannels for molecular sequence determination.[18] The challenge for computational molecular modeling for these systems is maintaining the molecular detail necessary to describe relatively complex behavior along with the relatively long times that are necessary for a realistic description of the phenomena.

In previous papers, we have developed a formal, statistical mechanics approach to describe the long-time dynamics of rigid macromolecules in the presence of external surfaces including the detailed molecular structure of the particle and surface.[19–21] The method is based on a molecular derivation of the Fokker–Planck (FP) equation that describes in a general fashion the dynamics of Brownian particles in a host solvent. We demonstrated that important effects associated with solvent averaging in the presence of an external surface are systematically accounted for by the FP equation; these include the so-called hydrodynamic interactions between the particle and surface, hydrophobic effects due to the specific solvent molecular configurations in the system, and configurationally dependent solvent dielectric effects.

Fundamentally, the Fokker-Planck equation is equivalent to the so-called Langevin equation, and either may be used to derive a phase-space (momentum and configuration) finite-difference, displacement equation for use in applications.[22,23] The computational technique has also been termed *coarse-grained molecular dynamics* due to the averaging process that takes place over the solvent phase (implicit solvent methods) and the retention of the molecular structure and forces associated with the rigid elements.[24–28] The parameters of the FP or Langevin equation are determined via separate molecular dynamic studies, correlation methods, and/or analytical

a)Electronic mail: mpeters@vcu.edu.

approximations.[1–7,24–31] The Langevin displacement equation allows relatively larger time steps than molecular dynamics, usually at least 2 orders of magnitude larger, and a significant reduction in the number of atoms to solely those of the particle and external surface, the latter as a result of the formal averaging process over the solvent phase.

Because of the practical need to computationally study flexible macromolecules in confined geometries for relatively long times, the analysis given here extends our previous theoretical studies to flexible macromolecules in the presence of fixed external surfaces. The flexibility, in this case, arises from a general set of interaction potentials between rigid, Brownian subunits of the macromolecule. In particular, we derive both a FP and associated Langevin displacement equation for these systems for use in applications including computations. The specific parameters of the FP and Langevin equation are shown to be physically transparent, and a prescription for their determination is provided that is critical to encompassing a wide range of applications. In addition, the formal scaling analysis that we utilize provides important physical limitations on the use of the FP and Langevin equations in any given system.

II. LIOUVILLE EQUATION

The Liouville equation provides the complete molecular description of the system dynamics in terms of a probability density function for finding all of the system molecules with particular positions and velocities at any time, t. We denote the entirety of generalized coordinates as $q = \{q_1, q_2, \ldots, q_s\}$, the associated conjugate momenta as $p = \{p_1, p_2, \ldots, p_s\}$, and a probability density function, f, in this multidimensional space as

$$f(q, p, t)dqdp,$$

which represents the number of occurrences or "phase points" of the system between (q, p) and $(q + dq, p + dp)$ at any time t. The total number of phase points must satisfy a simple conservation relation that can be written in terms of the total Hamiltonian, H, as

$$\frac{\partial f}{\partial t} = -\sum_{i=1}^{s}\left[\frac{\partial H}{\partial p_i}\frac{\partial f}{\partial q_i} - \frac{\partial H}{\partial q_i}\frac{\partial f}{\partial p_i}\right]. \tag{1}$$

Now, consider the generalized coordinates necessary for the description of M interacting, structured Brownian particles in a host solvent, including an external, structured surface as depicted in Fig. 1 and given explicitly as

$$(q, p) \equiv (\mathbf{r}^N, \mathbf{p}^N, \mathbf{R}^M, \Omega^M, \mathbf{P}^M, \mathbf{P}_\Omega^M). \tag{2}$$

Here $(\mathbf{r}^N, \mathbf{p}^N)$ refer to the position and momentum set of solvent molecules $(\mathbf{r}_1, \mathbf{r}_2, ..., \mathbf{r}_N, \mathbf{p}_1, \mathbf{p}_2, ..., \mathbf{p}_N)$, and $(\mathbf{R}^M, \mathbf{P}^M)$ represent the center of mass positions and momenta of the B(Brownian)-particles. Also, Ω^M and $\mathbf{P}_\Omega^M$ are short-hand notation for the set of Euler angles or their equivalent $(\phi_1, \psi_1, \theta_1, ..., \phi_M, \psi_M, \theta_M)$ and associated conjugate momenta $(P_{\phi_1}, P_{\psi_1}, P_{\theta_1}, ..., P_{\phi_M}, P_{\psi_M}, P_{\theta_M})$ for B-particles, respectively; it is to be understood that these are not vectors in the usual sense. For our system, assuming pairwise additivity

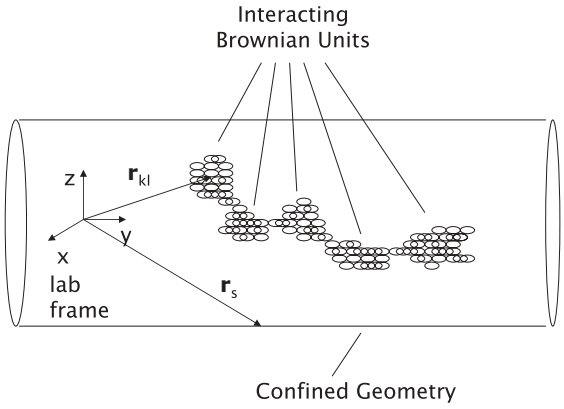

FIG. 1. Example illustration and notation for interacting Brownian particles in a confined geometry.

of the interaction forces, the Hamiltonian or total energy can be expressed as

$$\begin{aligned} H = T &+ \sum_{i=1}^{N}\sum_{\substack{j=1\\ j<i}}^{N} u_{ff}(\mathbf{r}_i, \mathbf{r}_j) \\ &+ \sum_{i=1}^{N}\sum_{l=1}^{M}\sum_{k_l} u_{fp}(\mathbf{r}_i, \mathbf{R}_l, \Omega_l; \bar{\mathbf{a}}_{k_l}) \\ &+ \sum_{i=1}^{N}\sum_{s} u_{fw}(|\mathbf{r}_i - \mathbf{r}_s|) \\ &+ \sum_{l=1}^{M}\sum_{k_l}\sum_{s} u_{p\omega}(\mathbf{r}_s, \mathbf{R}_l, \Omega_l; \bar{\mathbf{a}}_{k_l}) \\ &+ \sum_{l=1}^{M}\sum_{k_l}\left[\sum_{\substack{m=1\\ m<l}}^{M}\sum_{k_m} u_{pp}(\mathbf{R}_l, \mathbf{R}_m, \Omega_l, \Omega_m; \bar{\mathbf{a}}_{k_l}, \bar{\mathbf{a}}_{k_m})\right], \end{aligned} \tag{3}$$

where T is the total kinetic energy; u_{ff} is the solvent–solvent interaction potential; u_{fp} is the solvent–particle interaction potential; $u_{p\omega}$ is the particle–external surface interaction potential; u_{pp} is the particle–particle interaction potential. Note that the specific potential function expressions may vary depending on particle and solvent type. Also, $\mathbf{r}_i$ and $\mathbf{r}_j$ are location vectors for fluid molecules i and j, respectively, $\mathbf{r}_s$ is the location vector for the sth surface molecule, $\bar{\mathbf{a}}_{k_l}$ is the location vector of the kth molecule or atom of the lth B-particle in a frame of reference *fixed with respect to the B-particle* and with origin at the center of mass, $\mathbf{R}_l$ (see Fig. 1). The locator vectors $\bar{\mathbf{a}}_{k_l}$ are constants and fix the particular molecular structure of the lth B-particle; they are assumed known *a priori*.

The total kinetic energy, T, is given by the sum of the translational and rotational kinetic energies as

$$T = \sum_{i=1}^{N}\frac{1}{2}\frac{p_i^2}{m_i} + \sum_{l=1}^{M}\left[\frac{1}{2}\frac{P_l^2}{M_l} + T_{\mathrm{rot}_l}\right], \tag{4}$$

where m_i is the mass of the ith solvent molecule, M_l is the mass of the lth B-particle, and the rotational kinetic energy of

the lth B-particle can be expressed in terms of the generalized momenta as[19]

$$T_{\mathrm{rot}_l} = \frac{1}{2}\frac{1}{I_{\bar{1}_l}\sin^2\theta_l}[\sin\psi_l(P_{\phi_l} - \cos\theta_l P_{\psi_l}) + \cos\psi_l \sin\theta_l P_{\theta_l}]^2$$

$$+\frac{1}{2}\frac{1}{I_{\bar{2}_l}\sin^2\theta_l}[\cos\psi_l(P_{\phi_l} - \cos\theta_l P_{\psi_l}) - \sin\psi_l \sin\theta_l P_{\theta_l}]^2$$

$$+\frac{1}{2}\frac{1}{I_{\bar{3}_l}}P_{\psi_l}^2, \tag{5}$$

where the principal moment $I_{\bar{i}_l}$ is the $\bar{i}$th component of the moment of inertia of the lth B-particle in the body-fixed frame. Note that the principal moments of inertia are assumed constant for each B-particle. The functional dependencies shown for the interaction potentials can be seen as follows. For example, we have that (Fig. 1)

$$u_{fp} = u_{fp}(|\mathbf{r}_i - (\mathbf{a}_{k_l} + \mathbf{R}_l)|), \tag{6}$$

where $\mathbf{a}_{k_l}$ is the locator vector with respect to the laboratory frame. Relative to the lth B-particle frame, we have

$$\mathbf{a}_{k_l} = \mathbf{S}_l \cdot \bar{\mathbf{a}}_{k_l}, \tag{7}$$

where $\mathbf{S}_l$ is the transformation matrix that relates the locator vector of the lth B-particle frame, $\bar{\mathbf{a}}_{k_l}$, to the laboratory or inertial frame, $\mathbf{a}_{k_l}$. Now, $\mathbf{S}_l$ depends explicitly on the Euler angles or their equivalent, i.e., in component notation

$$a_{k_{l_i}} = \sum_{\bar{j}} e_{l_{i\bar{j}}} \bar{a}_{k_{l_{\bar{j}}}} \tag{8}$$

and the transformation matrix is given by[19]

$$[e_{l_{i\bar{j}}}] = \begin{bmatrix} \cos\phi_l \cos\psi_l - \sin\phi_l \cos\theta_l \sin\psi_l & -\cos\phi_l \sin\psi_l - \sin\phi_l \cos\theta_l \cos\psi_l & \sin\phi_l \sin\theta_l \\ \sin\phi_l \cos\psi_l + \cos\phi_l \cos\theta_l \sin\psi_l & -\sin\phi_l \sin\psi_l + \cos\phi_l \cos\theta_l \cos\psi_l & -\cos\phi_l \sin\theta_l \\ \sin\theta_l \sin\psi_l & \sin\theta_l \cos\psi_l & \cos\theta_l \end{bmatrix}. \tag{9}$$

Because each B-particle is assumed rigid, the locator vectors, $\bar{\mathbf{a}}_{k_l}$, in the lth B-particle frame are constants. Thus, we can write that

$$u_{fp} = u_{fp}(\mathbf{r}_i, \mathbf{R}_l, \Omega_l; \bar{\mathbf{a}}_{k_l}). \tag{10}$$

A similar analysis applies to $u_{p\omega}$ and u_{pp}, and their functional dependencies follow as shown in Eq. (3). Note that other external field potentials, such as electrical potentials that "drive" charged particles, can be included with the u_{pp} term.

III. FOKKER–PLANCK EQUATION

To formally obtain the FP equation for this system, a multiple time scale analysis of the Liouville equation is developed.[19,32–34] First, the Liouville equation is nondimensionalized or scaled to obtain[19]

$$\frac{\partial f^*}{\partial t^*} = (-N_{Kn}^{-1} L_f^* + \gamma L_p^*) f^*, \tag{11}$$

where $N_{Kn} = r_0/R_0$,$\gamma = m/M$, and L_f^* and L_p^* are particular nondimensional Liouville operators for this system, and the $*$ indicates a dimensionless variable. In the Knudsen number definition, r_0 is a characteristic length scale for the fluid intermolecular interaction force and, for an isolated Brownian particle, R_0 is a characteristic length scale for the interaction force between the macromolecule and the fluid, often taken as the effective overall macromolecular diameter. Fundamentally, R_0 is the length scale over which the potential of force acting on a B-particle changes by order of kT. This force also includes particle–particle forces and particle–wall forces. This length scale is important in establishing existence of what is called a Markov-type FP equation that will be obtained below.[19] In addition, another important parameter, shown below, is the mass ratio term $\gamma = m/M$, where M is a characteristic mass for the B-particles and m is a characteristic mass of a solvent molecule.

The nondimensional Liouville operators L_f^* and L_p^* for this system are defined as

$$L_f^* = \sum_{i=1}^{N}\left[\mathbf{p}_i^* \cdot \frac{\partial}{\partial \mathbf{r}_i^*}\left(\sum_{\substack{j=1\\ j<i}}^{N} u_{ff}^* + \sum_{l=1}^{M}\sum_{k_l} u_{fp}^* + \sum_{s} u_{fw}^*\right) \cdot \frac{\partial}{\partial \mathbf{p}_i^*}\right] \tag{12}$$

$$L_p^* = \sum_{l=1}^{M}\left[\mathbf{P}_l^* \cdot \frac{\partial}{\partial \mathbf{R}_l^*} + \frac{\partial T_{rot_l}^*}{\partial \mathbf{P}_{\Omega_l}^*} \cdot \frac{\partial}{\partial \Omega_{\mathbf{l}}} - \frac{\partial T_{rot_l}^*}{\partial \Omega_l} \cdot \frac{\partial}{\partial \mathbf{P}_{\Omega_l}^*}\right.$$

$$-\frac{\partial}{\partial \mathbf{R}_l^*}\left(\sum_{i=1}^{N}\sum_{k_l} u_{fp}^* + \sum_{k_l}\sum_{s} u_{p\omega}^* + \sum_{k_l}\sum_{\substack{m=1\\ m<l}}^{M}\sum_{k_m} u_{pp}^*\right) \cdot \frac{\partial}{\partial \mathbf{P}_l^*}$$

$$-\frac{\partial}{\partial \Omega_l}\left(\sum_{i=1}^{N}\sum_{k_l} u_{fp}^* + \sum_{k_l}\sum_{s} u_{p\omega}^* + \sum_{k_l}\sum_{\substack{m=1\\ m<l}}^{M}\sum_{k_m} u_{pp}^*\right) \cdot \left.\frac{\partial}{\partial \mathbf{P}_{\Omega_l}^*}\right]. \tag{13}$$

We also introduce the reduced or contracted distribution function for the B-particles only as

$$\Psi(\mathbf{R}^M, \mathbf{P}^M, \Omega^M, \mathbf{P}_\Omega^M, t) = \int_{\text{all}\mathbf{r}^N, \mathbf{p}^N} f(\mathbf{r}^N, \mathbf{p}^N, \mathbf{R}^M, \mathbf{P}^M, \Omega^M, \mathbf{P}_\Omega^M, t) d\mathbf{r}^N d\mathbf{p}^N. \quad (14)$$

Now, the mass ratio is typically very small so that the distribution function can be expanded in terms of γ and introducing multiple time scales ($\tau_0, \tau_1, \tau_2, \ldots$), we can write [19,32–34]

$$f^* = f^*(\mathbf{r}^N, \mathbf{p}^N, \mathbf{R}^M, \mathbf{P}^M, \Omega^M, \mathbf{P}_\Omega^M, \tau_0, \tau_1, \tau_2, \ldots) = f^{*(0)} + \gamma f^{*(1)} + \gamma^2 f^{*(2)} + \cdots \quad (15)$$

The expansion procedure has been presented in detail previously[19] and only the final results are given here for the sake of brevity. In general, the expansion is conducted through second order in mass ratio and time scales, leading to a Fokker–Planck equation for the total space-time behavior of the contracted distribution function for the B-particles, written in dimensional form as

$$\begin{aligned}
&\frac{\partial \Psi}{\partial t} + \sum_{l=1}^{M} \left\{ \frac{\mathbf{P}_l}{M_l} \cdot \frac{\partial \Psi}{\partial \mathbf{R}_l} + \left[\langle \mathbf{F}_{f_l} \rangle_{eq} \right.\right. \\
&\quad \left. - \frac{\partial}{\partial \mathbf{R}_l} \left(\sum_{k_l} \sum_{s} u_{p\omega} + \sum_{k_l} \sum_{\substack{m=1 \\ m<l}}^{M} \sum_{k_m} u_{pp} \right) \right] \cdot \frac{\partial \Psi}{\partial \mathbf{P}_l} \\
&\quad + \frac{\partial T_{rot_l}}{\partial \mathbf{P}_{\Omega_l}} \cdot \frac{\partial \Psi}{\partial \Omega_l} + \left[\langle \mathbf{T}_{f_l} \rangle_{eq} - \frac{\partial}{\partial \Omega_l} \left(T_{rot_l} \right.\right. \\
&\quad \left.\left. + \sum_{k_l} \sum_{s} u_{p\omega} + \sum_{k_l} \sum_{\substack{m=1 \\ m<l}}^{M} \sum_{k_m} u_{pp} \right) \right] \cdot \frac{\partial \Psi}{\partial \mathbf{P}_{\Omega_l}} \Bigg\} \\
&= kT \sum_{l=1}^{M} \left\{ \frac{\partial}{\partial \mathbf{P}_l} \cdot \left(\zeta_{T_l} \cdot \left[\Psi \frac{\mathbf{P}}{M_l kT} + \frac{\partial \Psi}{\partial \mathbf{P}_l} \right] \right.\right. \\
&\quad \left. + \zeta_{TR_l} \cdot \left[\Psi \frac{1}{kT} \frac{\partial T_{rot_l}}{\partial \mathbf{P}_{\Omega_l}} + \frac{\partial \Psi}{\partial \mathbf{P}_{\Omega_l}} \right] \right) \\
&\quad + \frac{\partial}{\partial \mathbf{P}_{\Omega_l}} \cdot \left(\zeta_{R_l} \cdot \left[\Psi \frac{1}{kT} \frac{\partial T_{rot_l}}{\partial \mathbf{P}_{\Omega_l}} + \frac{\partial \Psi}{\partial \mathbf{P}_{\Omega_l}} \right] \right. \\
&\quad \left.\left. + \zeta_{RT_l} \cdot \left[\Psi \frac{\mathbf{P}_l}{M_l kT} + \frac{\partial \Psi}{\partial \mathbf{P}_l} \right] \right) \right\}, \quad (16)
\end{aligned}$$

where k is Boltzmann's constant, T is absolute temperature, and T_{rot_l} is the rotational kinetic energy of the lth B-particle given by Eq. (6). The force and torque acting on the lth B-particle by the fluid are defined, respectively, by

$$\mathbf{F}_{f_l} \equiv -\frac{\partial}{\partial \mathbf{R}_l} \left[\sum_{i=1}^{N} \sum_{k_l} u_{fp} \right], \quad (17)$$

$$\mathbf{T}_{f_l} \equiv -\frac{\partial}{\partial \Omega_l} \left[\sum_{i=1}^{N} \sum_{k_l} u_{fp} \right]. \quad (18)$$

Further, $\langle \mathbf{F}_{f_l} \rangle_{\text{eq}}$ and $\langle \mathbf{T}_{f_l} \rangle_{\text{eq}}$ are the equilibrium average force and torque, respectively, acting on the lth B-particle by the fluid. The equilibrium averages are defined as

$$\langle A \rangle_{\text{eq}} \equiv \int_{\text{all}\mathbf{r}^N, \mathbf{p}^N} A \times h_{\text{eq}}(\mathbf{r}^N, \mathbf{p}^N; \mathbf{R}^M, \mathbf{P}^M, \Omega^M, \mathbf{P}_\Omega^M, t) d\mathbf{r}^N d\mathbf{p}^N, \quad (19)$$

where h_{eq} is a marginal or conditional local fluid equilibrium distribution function with given variables for the B-particles and in the presence of an external surface.[19] For an isolated B-particle, the local equilibrium force and torque acting on the particle by the fluid vanish, but they are finite when other B-particles or surfaces are present.[19] Nonequilibrium local fluid distribution functions have also been included, such as those due to bulk fluid flow or external forces.[35,36] Note that the equilibrium fluid force acting on the B-particles can often be broken down into different contributions depending on the nature of the interaction potential. For example, an electrostatic force interaction between a polar solvent, such as water, and the B-particles leads to the local dielectric behavior of the fluid in the configuration space of the B-particles, and the accompanying nonpolar force interactions, such as van der Waals and Born force interactions, lead to the so-called hydrophobic effect.

The translational, rotational, and coupled translational–rotational friction tensors in Eq. (16) are defined by

$$\zeta_{T_l} \equiv \frac{1}{kT} \int_0^\infty [\langle \mathbf{F}_{f_l}(s) \mathbf{F}_{f_l}(0) \rangle_{\text{eq}} - \langle \mathbf{F}_{f_l} \rangle_{\text{eq}}^2] ds, \quad (20)$$

$$\zeta_{TR_l} \equiv \frac{1}{kT} \int_0^\infty [\langle \mathbf{F}_{f_l}(s) \mathbf{T}_{f_l}(0) \rangle_{\text{eq}} - \langle \mathbf{F}_{f_l} \rangle_{\text{eq}} \langle \mathbf{T}_{f_l} \rangle_{\text{eq}}] ds, \quad (21)$$

$$\zeta_{RT_l} \equiv \frac{1}{kT} \int_0^\infty [\langle \mathbf{T}_{f_l}(s) \mathbf{F}_{f_l}(0) \rangle_{\text{eq}} - \langle \mathbf{T}_{f_l} \rangle_{\text{eq}} \langle \mathbf{F}_{f_l} \rangle_{\text{eq}}] ds, \quad (22)$$

$$\zeta_{R_l} \equiv \frac{1}{kT} \int_0^\infty [\langle \mathbf{T}_{f_l}(s) \mathbf{T}_{f_l}(0) \rangle_{\text{eq}} - \langle \mathbf{T}_{f_l} \rangle_{\text{eq}}^2] ds. \quad (23)$$

Note that the friction tensors, Eqs. (20)–(23), will depend on the separation distance and orientation of the lth B-particle with respect to other B-particles and surfaces present. In continuum fluid mechanics, this latter effect is known as "hydrodynamic interactions." In general, the friction tensors can be determined from the above integrals through equilibrium canonical molecular dynamics for any given B-particles' positions and orientations in the system. Equations (16)–(23) are the central result of the Brownian approximation for this system. The host fluid must quickly relax to the potential field created by the B-particles; a condition that exists for small Knudsen numbers, $N_{Kn} << 1$. Mathematically, the integrals in Eqs. (20)–(23) converge rapidly under these conditions, and the friction tensors are referred to as "memoryless" and the associated FP equation is referred to as "classical" or Markovian.[37] Note that during the short-time solvent relaxation period, there can be no significant change in the B-particles' positions or orientations.

Now, the numerical or finite-difference solution to the FP equation leads to a Brownian dynamics (BD) algorithm, or long-time, BD time step, for determining the macromolecular

displacements.[22,23] In deriving finite difference forms for use in applications, it is useful to express the FP equation in terms of the angular momenta in the laboratory frame, $\mathbf{L}$, rather than the conjugate momenta, $\mathbf{P}_\Omega$. The transformations have been presented in detail previously, and here we simply present the results for the sake of brevity.[20] Accordingly, the FP equation can be re-expressed in terms of angular momentum as

$$\frac{\mathcal{D}\Psi}{\mathcal{D}t} = kT\sum_{l=1}^{M}\left\{\left[\mathbf{G}_{p_l}\ \mathbf{G}_{L_l}\right]\begin{bmatrix}\zeta_{T_l} & \zeta_{TR_l}\\ \zeta_{RT_l} & \zeta_{R_l}\end{bmatrix}\begin{bmatrix}\mathbf{Q}_{p_l}\Psi\\ \mathbf{Q}_{L_l}\Psi\end{bmatrix}\right\}, \tag{24}$$

where

$$\frac{\mathcal{D}}{\mathcal{D}t} \equiv \frac{\partial}{\partial t} + \sum_{l=1}^{M}\left[\frac{\mathbf{P}_l}{M_l}\cdot\frac{\partial}{\partial \mathbf{R}_l} + \mathbf{F}'_l\cdot\frac{\partial}{\partial \mathbf{P}_l} + \omega_{1_l}\frac{\partial}{\partial\phi_{1_l}} + \omega_{2_l}\frac{\partial}{\partial\phi_{2_l}} + \omega_{3_l}\frac{\partial}{\partial\phi_{3_l}} + T'_{1_l}\frac{\partial}{\partial L_{1_l}} + T'_{2_l}\frac{\partial}{\partial L_{2_l}} + T'_{3_l}\frac{\partial}{\partial L_{3_l}}\right], \tag{25}$$

$$\mathbf{G}_{p_l} \equiv \frac{\partial}{\partial \mathbf{P}_l}, \tag{26}$$

$$\mathbf{G}_{L_l} \equiv \frac{\partial}{\partial \mathbf{L}_l}, \tag{27}$$

$$\mathbf{Q}_{p_l} \equiv \frac{\mathbf{P}_l}{M_l kT} + \frac{\partial}{\partial \mathbf{P}_l}, \tag{28}$$

$$\mathbf{Q}_{L_l} \equiv \frac{\omega_l}{kT} + \frac{\partial}{\partial \mathbf{L}_l}, \tag{29}$$

and

$$\mathbf{F}'_l \equiv \langle \mathbf{F}_{f_l}\rangle_{\mathrm{eq}} - \frac{\partial}{\partial \mathbf{R}_l}\left(\sum_{k_l}\sum_{s} u_{p\omega} + \sum_{k_l}\sum_{\substack{m=1\\ m<l}}^{M}\sum_{k_m} u_{pp}\right), \tag{30}$$

$$\mathbf{T}'_l \equiv (T'_{\theta_l}, T'_{\phi_l}, T'_{\psi_l}) \equiv \langle \mathbf{T}_{f_l}\rangle_{\mathrm{eq}} - \frac{\partial}{\partial \mathbf{\Omega}_l}\left(\sum_{k_l}\sum_{s} u_{p\omega} + \sum_{k_l}\sum_{\substack{m=1\\ m<l}}^{M}\sum_{k_m} u_{pp}\right). \tag{31}$$

Note that it is understood that the angular velocities, ω_l, in the laboratory frame are to be expressed in terms of the angular momentum as

$$\omega_l \equiv \mathbf{L}_l\cdot\mathbf{I}_l^{-1}, \tag{32}$$

where $\mathbf{I}_l$ is the moment of inertia tensor for the lth Brownian particle expressed in the laboratory frame. Also, note that $(\omega_{1_l}, \omega_{2_l}, \omega_{3_l})$ and $(T'_{1_l}, T'_{2_l}, T'_{3_l})$ appearing in Eq. (25) are the Cartesian components of the angular velocity and torque, respectively, in the space-fixed or laboratory frame. The Cartesian components are related to the $(\theta_l, \phi_l, \psi_l)$ components given in Eq. (31) above as[20]

$$T_{1_l} = T_{\theta_l}\cos\phi_l - T_{\phi_l}\cot\theta_l\sin\phi_l + T_{\psi_l}\csc\theta_l\sin\phi_l, \tag{33}$$

$$T_{2_l} = T_{\theta_l}\sin\phi_l + T_{\phi_l}\cot\theta_l\cos\phi_l - T_{\psi_l}\csc\theta_l\cos\phi_l, \tag{34}$$

$$T_{3_l} = T_{\phi_l}. \tag{35}$$

We have also used the transformation relations between the Euler angles and rotations about the Cartesian frame as[20]

$$\frac{\partial}{\partial\phi_{1_l}} = \cos\phi_l\frac{\partial}{\partial\theta_l} - \cot\theta_l\sin\phi_l\frac{\partial}{\partial\phi_l} + \csc\theta_l\sin\phi_l\frac{\partial}{\partial\psi_l}, \tag{36}$$

$$\frac{\partial}{\partial\phi_{2_l}} = \sin\phi_l\frac{\partial}{\partial\theta_l} + \cot\theta_l\cos\phi_l\frac{\partial}{\partial\phi_l} - \csc\theta_l\cos\phi_l\frac{\partial}{\partial\psi_l}, \tag{37}$$

$$\frac{\partial}{\partial\phi_{3_l}} = \frac{\partial}{\partial\phi_l}. \tag{38}$$

The friction tensors in Eq. (25) are now given completely in the space-fixed Cartesian frame. For example,

$$\zeta_{RT} \doteq \begin{bmatrix}\zeta_{RT_{11_l}} & \zeta_{RT_{12_l}} & \zeta_{RT_{13_l}}\\ \zeta_{RT_{21_l}} & \zeta_{RT_{22_l}} & \zeta_{RT_{23_l}}\\ \zeta_{RT_{31_l}} & \zeta_{RT_{32_l}} & \zeta_{RT_{33_l}}\end{bmatrix}, \tag{39}$$

where the x–x component is

$$\zeta_{RT_{11_l}} \equiv \int_0^\infty [\langle T_{1_{f_l}}(0)F_{1_{f_l}}(s)\rangle_{\mathrm{eq}} - \langle T_{1_{f_l}}\rangle_{\mathrm{eq}}\langle F_{1_{f_l}}\rangle_{\mathrm{eq}}]ds, \tag{40}$$

etc. For an isolated B-particle, Eq. (25) is in agreement with the FP equation given by Condiff and Dahler.[38]

IV. SMOLUCHOWSKI AND LANGEVIN DISPLACEMENT EQUATIONS

Now, we will derive the short-time solution to the FP equation that leads to the finite difference form of the associated Langevin equation as shown by Ermak and McCammon.[22] First, we define the following dimensionless variables based on the B-particle characteristics and denoted by asterisk symbols as

$$\Psi = \Psi^*\frac{n_0}{(R_0MkT)^{3l}}, \tag{41}$$

$$\mathbf{P}_l = \mathbf{P}_l^*(MkT)^{1/2}, \tag{42}$$

$$\mathbf{R}_l = \mathbf{R}_l^* R_0, \tag{43}$$

$$t = t^*t_0 = t^*[R_0/(kT/M)^{1/2}], \tag{44}$$

$$\mathbf{L}_l = \mathbf{L}_l^* R_0(MkT)^{1/2}, \tag{45}$$

$$\omega_l = \omega_l^*[(kT/M)^{1/2}/R_0], \tag{46}$$

$$\mathbf{F}'_l = \mathbf{F}'^*_l(kT/R_0), \tag{47}$$

$$\mathbf{T}'_l = \mathbf{T}'^*_l(kT), \tag{48}$$

$$\zeta_{T_l} = \zeta^*_{T_l}\zeta_0, \tag{49}$$

$$\zeta_{TR_l} = \zeta^*_{TR_l}R_0\zeta_0, \tag{50}$$

$$\zeta_{RT_l} = \zeta^*_{RT_l} R_0 \zeta_0, \tag{51}$$

$$\zeta_{R_l} = \zeta^*_{R_l} R_0^2 \zeta_0. \tag{52}$$

Substituting the dimensionless variables into the FP equation, Eq. (24), yields

$$\frac{\mathcal{D}^*\Psi^*}{\mathcal{D}^* t^*} = \frac{1}{N_{\mathrm{St}}} \sum_{l=1}^{M} \left\{ \begin{bmatrix} \mathbf{G}^*_{P_l} & \mathbf{G}^*_{L_l} \end{bmatrix} \times \begin{bmatrix} \zeta^*_{T_l} & \zeta^*_{TR_l} \\ \zeta^*_{RT_l} & \zeta^*_{R_l} \end{bmatrix} \begin{bmatrix} \mathcal{Q}^*_{P_l} \Psi^* \\ \mathcal{Q}^*_{L_l} \Psi^* \end{bmatrix} \right\}, \tag{53}$$

where N_{St} is the particle Stokes number

$$N_{\mathrm{St}} = \frac{\zeta_0^{-1} M}{R_0/(kT/M)^{1/2}} = \frac{t_{\mathrm{relax}}}{t_0}. \tag{54}$$

The particle Stokes number is the ratio of the particle relaxation time, $\zeta_0^{-1} M$, to the characteristic time constant, t_0. The particle Stokes number is important in establishing conditions of the diffusion or Smoluchowski limit of the FP equation, as shown below.

Now, because of the highly coupled nature of linear and angular momenta for this problem, some approximations are necessary, even for small times, to effect solutions of the FP equation. These approximations include: 1) isotropic particle assumptions where linear and angular momenta can be decoupled[39] and 2) Stokes number expansions where particle inertial effects are small. As pointed out by Harris,[39] any isotropy assumption is only required to be within the order of the mass ratio expansion, and therefore, the terminology "nearly isotropic" is more appropriate. Expansion of the FP equation in Stokes number leads to the diffusion limit or Smoluchowski equation, as shown previously by Dickinson *et al.*[23] for interacting Brownian particles. The Stokes number expansion solution to the FP equation has been presented in detail previously,[20] and here we simply present the essential results for the sake of brevity.

For small Stokes numbers, we seek a solution for the configurational–orientational distribution function defined as

$$n^*(\mathbf{R}^{*M}, \mathbf{\Phi}^M, t^*) = \int \int \Psi^* d\mathbf{P}^{*M} d\mathbf{L}^{*M} \tag{55}$$

and we write the expansion solution as

$$\Psi^* = \sum_{n=0}^{\infty} \epsilon^n \Psi^{*(n)}, \ \epsilon \to 0+. \tag{56}$$

Substituting Eq. (56) into Eq. (53) leads to the following problems:

$$0(\epsilon^\circ): \sum_{l=1}^{M} \left\{ \begin{bmatrix} \mathbf{G}^*_{P_l} & \mathbf{G}^*_{L_l} \end{bmatrix} \begin{bmatrix} \zeta^*_{T_l} & \zeta^*_{TR_l} \\ \zeta^*_{RT_l} & \zeta^*_{R_l} \end{bmatrix} \begin{bmatrix} \mathcal{Q}^*_{P_l} \Psi^{*(0)} \\ \mathcal{Q}^*_{L_l} \Psi^{*(0)} \end{bmatrix} \right\} = 0 \tag{57}$$

$$0(\epsilon'): \frac{\mathcal{D}\Psi^{(0)}}{\mathcal{D}t} = \sum_{l=1}^{M} \left\{ \begin{bmatrix} \mathbf{G}^*_{P_l} & \mathbf{G}^*_{L_l} \end{bmatrix} \begin{bmatrix} \zeta^*_{T_l} & \zeta^*_{TR_l} \\ \zeta^*_{RT_l} & \zeta^*_{R_l} \end{bmatrix} \begin{bmatrix} \mathcal{Q}^*_{P_l} \Psi^{*(1)} \\ \mathcal{Q}^*_{L_l} \Psi^{*(1)} \end{bmatrix} \right\}. \tag{58}$$

Now, following the steps given previously, the Smoluchowski equation is obtained as[20]

$$\frac{\partial n}{\partial t} = \epsilon \sum_{l=1}^{M} [\partial/\partial \mathbf{R}_l \ \partial/\partial \mathbf{\Phi}_l] \begin{bmatrix} \mathbf{D}_{T_l} & \mathbf{D}_{TR_l} \\ \mathbf{D}_{RT_l} & \mathbf{D}_{R_l} \end{bmatrix} \times \begin{bmatrix} \partial n/\partial \mathbf{R}_l - n\mathbf{F}'_l \\ \partial n/\partial \mathbf{\Phi}_l - n\mathbf{T}'_l \end{bmatrix} + 0(\epsilon^2), \tag{59}$$

where we have dropped the asterisk notation for the sake of simplicity. A Brownian dynamics or numerical solution to the Smoluchowski equation can be obtained by deriving an analytical solution for its short-time behavior. In doing this, we consider that at time $t = 0$, the positions and orientations of the B-particles are exactly known, i.e.,

$$n = \prod_l \delta(\mathbf{R}_l - \mathbf{R}^0_l)\delta(\mathbf{\Phi}_l - \mathbf{\Phi}^0_l), \ \text{at} \ t = 0, \tag{60}$$

where δ is the Dirac delta function. Now for very small times t ($t > 0$), we can assume that all spatial and orientational functions are approximately constant at their initial values, i.e.,

$$\mathbf{F}'_l \cong \mathbf{F}'^0_l, \tag{61}$$

$$\mathbf{T}'_l \cong \mathbf{T}'^0_l, \tag{62}$$

$$\mathbf{D}_{J_l} \cong \mathbf{D}^0_{J_l}, \ J = T, TR, RT, R, \tag{63}$$

etc., where the superscript (0) indicates the known initial values. The solution to Eq. (53) under these conditions can be readily obtained as[20]

$$n(\mathbf{q}^M, t) = \prod_l \frac{1}{(4\pi t\epsilon)^3 Det[\mathbf{D}^0_l]^{1/2}} \times \exp\left\{ -\frac{1}{4t\epsilon} [\mathbf{q}_l - \mathbf{q}^0_l][\mathbf{D}^0_l]^{-1} [\mathbf{q}_l - \mathbf{q}^0_l]^\dagger \right\}, \tag{64}$$

where $\mathbf{q}_l \equiv (\mathbf{R}_l \oplus \mathbf{\Phi}_l)$ is a (1×6) vector and the 6×6 grand diffusion tensor, $\mathbf{D}^0_l$, is defined by

$$[\mathbf{D}^0_l] \equiv \begin{bmatrix} \mathbf{D}^0_{T_l} & \mathbf{D}^0_{TR_l} \\ \mathbf{D}^0_{RT_l} & \mathbf{D}^0_{R_l} \end{bmatrix}. \tag{65}$$

For each B-particle, Eq. (64) represents a multivariate Gaussian function with mean $\mathbf{q}^0_l$ and variance–covariance

$$\langle C_{i_l}(D^0_{i j_l}, t) C_{j_l}(D^0_{i j_l}, t) \rangle = 2 D^0_{i j_l} t\epsilon. \tag{66}$$

Finally, following Ermak and McCammon,[22] we can use Eqs. (64) and (66) to put the solution in the form of translational and rotational displacement equations for the lth B-particle as

$$R_{i_l} = R^0_{i_l} + \epsilon t \left[\sum_j (D^0_{i j_{T_l}} F'^0_{j_l} + D^0_{i j_{TR_l}} T'^0_{j_l}) \right] + C_{i_l}(D^0_{i j_l}, t), \ (1 \le i \le 3, \ 1 \le j \le 6), \tag{67}$$

$$\phi_{i_l} = \phi^0_{i_l} + \epsilon t \left[\sum_j (D^0_{i j_{RT_l}} F'^0_{j_l} + D^0_{i j_{R_l}} T'^0_{j_l}) \right] + C_{i_l}(D^0_{i j_l}, t), \ (4 \le i \le 6, \ 1 \le j \le 6), \tag{68}$$

where $C_{i_l}(D^0_{i_j l}, t)$ is a multivariate, Gaussian random number with zero mean and variance-covariance given by Eq. (66).

The general BD algorithm given above for confined systems is still relatively straightforward. The body-fixed molecular structure and potentials of the interacting B-particles and confining surfaces are specified. The implicit effects of the solvent are apparent through: 1) the definition of the diffusion tensors as proportional to the inverse friction tensors, Eqs. (20)–(23), and 2) the equilibrium average force and torques acting on the lth B-particle by the solvent, as given in Eqs. (19), (30), and (31). Specifically, using the marginal, local fluid equilibrium distribution function developed previously[19], we can write the local equilibrium average force and torque expressions as

$$\langle \mathbf{F}_{f_l} \rangle \equiv \int_{\text{all}\mathbf{r}^N,\mathbf{p}^N} \left\{ -\frac{\partial}{\partial \mathbf{R}_l} \left[\sum_{i=1}^{N} \sum_{k_l} u_{fp} \right] \right\} \times \exp[-H_f] d\mathbf{r}^N d\mathbf{p}^N \Big/ \int_{\text{all}\mathbf{r}^N,\mathbf{p}^N} \exp[-H_f] d\mathbf{r}^N d\mathbf{p}^N, \tag{69}$$

$$\langle \mathbf{T}_{f_l} \rangle \equiv \int_{\text{all}\mathbf{r}^N,\mathbf{p}^N} \left\{ -\frac{\partial}{\partial \Omega_l} \left[\sum_{i=1}^{N} \sum_{k_l} u_{fp} \right] \right\} \times \exp[-H_f] d\mathbf{r}^N d\mathbf{p}^N \Big/ \int_{\text{all}\mathbf{r}^N,\mathbf{p}^N} \exp[-H_f] d\mathbf{r}^N d\mathbf{p}^N, \tag{70}$$

where the fluid-side Hamiltonian is given from Eq. (3) as

$$H_f = \sum_{i=1}^{N} (1/2) p_i^2 / m_i + \sum_{i=1}^{N} \sum_{\substack{j=1 \\ j<i}}^{N} u_{ff}(\mathbf{r}_i, \mathbf{r}_j) + \sum_{i=1}^{N} \sum_{l=1}^{M} \sum_{k_l} u_{fp}(\mathbf{r}_i, \mathbf{R}_l, \Omega_l; \bar{\mathbf{a}}_{k_l}) + \sum_{i=1}^{N} \sum_{s} u_{fw}(|\mathbf{r}_i - \mathbf{r}_s|). \tag{71}$$

As an example, Roux and Simonson[40] and Wagoner and Baker[41] used the above equations, in the absence of confined geometries, to examine implicit solvation forces by further decomposing the interaction potentials in terms of polar (electrostatic) and nonpolar (Born repulsive and van der Waals) contributions. The above relations, Eqs. (69)–(71), allow for the study of polar and nonpolar solvation forces for interacting B-particles in confining geometries.

V. EXAMPLE APPLICATION: REAL-TIME MOTION OF A BIOLOGICAL MACROMOLECULE THROUGH A CARBON NANOTUBE

As discussed in Introduction, a contemporary application of biological macromolecular motion in confined geometries involves the threading of proteins or DNA through nanopores or nanochannels. Here we consider the movement of an α-helix protein through a carbon nanotube using the methodology developed above.

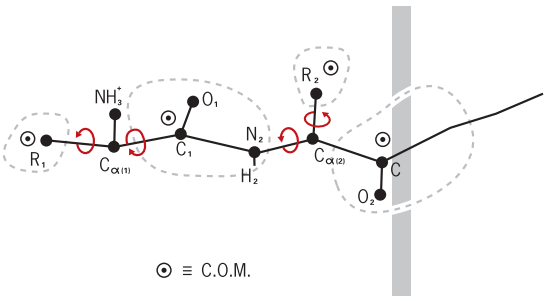

FIG. 2. Illustration of the structured Brownian subunits for protein macromolecules. Only the first (N-terminal) and second residues are shown.

In modeling proteins using BD methods, the protein is assumed to be comprised of structured, interacting rigid subunits. The protein model followed here was given previously by Wu and Sung[42] and is shown in Fig. 2. In this model, peptide bonds between $C_{(i)}$ and $N_{(i+1)}$ amino acids are considered to form rigid planar Brownian units (amide planes), where i denotes the amino acid residue number. Thus, the amide planes consist of atoms $O_{(i)}$, $C_{(i)}$, $N_{(i+1)}$, and $HN_{(i+1)}$. The side-chain groups, denoted by $R_{(i)}$, vary with each of the 20 types of amino acids and are also considered separate Brownian subunits as shown in Fig. 2. In the Wu and Sung model, the α-carbon is considered to be part of the R-group. For the sake of simplicity here, we consider the entire R-group to be a rigid subunit, although one could further divide R groups into specified rigid subunits depending on their structure and bonding behavior.[42] The α-carbon hydrogen is neglected in simulations in order to not artificially restrict the R-group rotational motions; it is added via geometric arguments for visualization purposes below. The amino-terminal group is included with the first residue R-group. The carboxy-terminal group constitutes the last Brownian subunit. The total number of Brownian units is, therefore, two times the total number of residues with the exception when Proline is present. Proline forms an expanded amide group with no R-group.

Now, it is necessary to maintain fixed bond distances and bond angles around each α-carbon that micromechanically constitutes a tetrahedral joint as shown in Fig. 3. Fixed bond distances and bond angles can be maintained by incorporating constraint equations into the algorithm, such as the SHAKE algorithm[43] used by Wu and Sung[42] and the LINCS

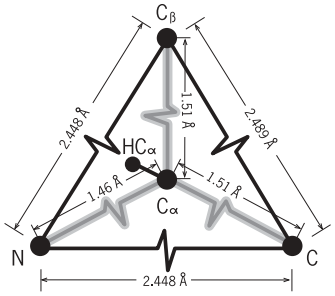

FIG. 3. Nomenclature and illustration of the tetrahedral joint associated with each α-carbon atom of the protein.

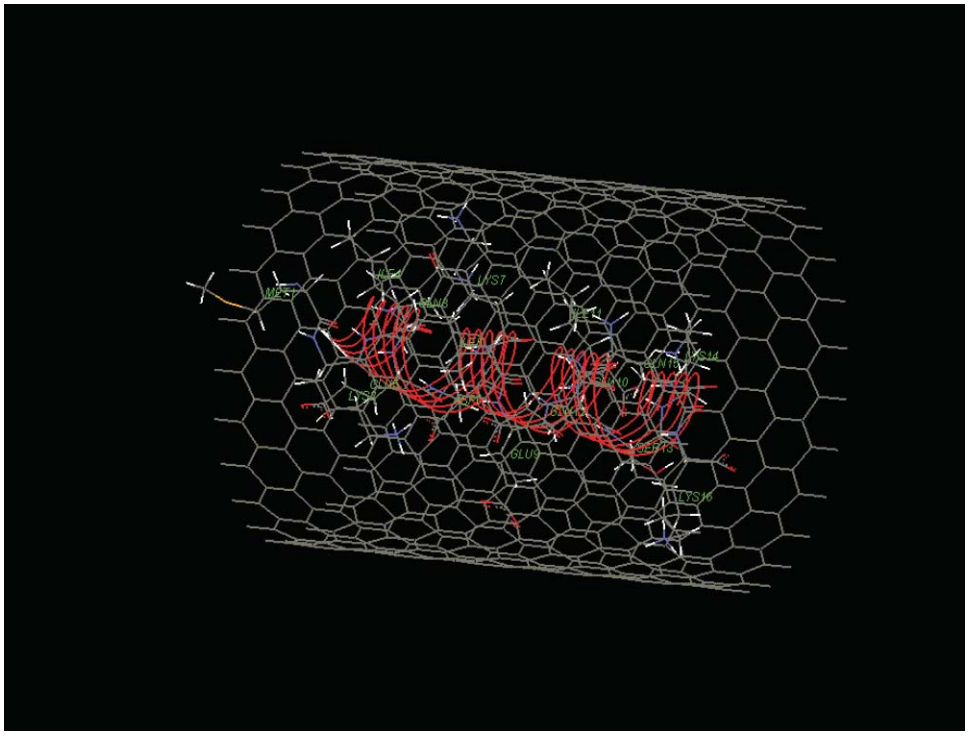

FIG. 4. $t = 0.0ns$. α- helix placed inside nanotube.

method[44] used, for example, by Ando *et al.*[45] and Shen *et al.*[2] in their atomistic BD simulations. Alternatively, following our previous studies,[46] we may employ "stiff" potential functions to approximately maintain fixed bond distances and angles. Specifically, for the tetrahedral joint, we can write for bond distances and bond angles, respectively,

$$U_l = \gamma_l (r_l - b_l)^2$$

$$U_k = \gamma_k (\alpha_k - \alpha_l)^2,$$

where the subscript l denotes the bond between two specified atoms of the joint and the subscript k denotes the angle between three specified atoms of the joint. Note that these potential functions are included in the u_{pp} terms of Eqs. (30) and (31) and lead to both forces and torques acting on each Brownian subunit attached to the joint. The specific constants employed in the simulations reported here are as follows:

$\angle C_\beta - C_\alpha - N\ \alpha_k = 109.7 \gamma_k = 400$ kcal/(mol radian^2)
$\angle C_\beta - C_\alpha - C\ \alpha_k = 111.0 \gamma_k = 315$ kcal/(mol radian^2)
$\angle N - C_\alpha - C\ \alpha_k = 110\ \gamma_k = 315$ kcal/(mol radian^2)
distance $C_\alpha - C\ b_l = 1.51$ Å $\gamma_l = 1585$ kcal/(mol Å^2)
distance $C_\alpha - N\ b_l = 1.46$ Å $\gamma_l = 1685$ kcal/(mol Å^2)
distance $C_\alpha - C_\beta\ b_l = 1.51$ Å$\gamma_l = 1560$ kcal/(mol Å^2).

In addition, we must maintain the positional relations between $C_{\alpha(i)} - C_{(i)}$ and $C_{\alpha(i)} - N_{(i)}$ bond vectors with their respective amide plane attachments. This requires, for example, that $C_{\alpha(i)} - C_{(i)}$ be equivalent to the vector that bisects $C_{(i)} - O_{(i)}$ and $C_{(i)} - N_{(i+1)}$ in the "downstream" amide plane. A similar argument applies to the $C_{\alpha(i)} - N_{(i)}$ bond vector with the "upstream" amide plane. Stiff potential functions are again used to maintain these positional relations (not shown here for the sake of brevity). The specific values for γ_k and γ_l given above were determined by trial-and-error as the approximate minimum values necessary to maintain the integrity of the protein structure in the absence of any external surfaces. They are approximately five times the soft potential values used in purely molecular dynamic algorithms.[47] Note that the stiff potential method for bond length and angle constraints is relatively easy and straightforward to implement in atomistic BD methods in general.

For all nonbonded potential functions between atoms we use AMBER force fields.[47] In this prescription all 1–2 and 1–3 nonbonded interactions are neglected, and 1–4 nonbonded interactions are scaled by 0.50. Dihedral potential functions were also used in the simulations following AMBER.[47]

The specific protein selected was an α-helical segment of the viral envelop protein of GP41[21]. The carbon nanotube molecular structure was generated using Nanotube Modeler (JCrystal Software Inc.). The specific parameters for the carbon nanotube generator were as follows:

Chirality (24,0)
Tube Length 25Å
Bond Length 1.41Å
MWNT 1,2,0.

These parameters resulted in a tube diameter of 18.657Å. The α-helix used in the simulations had an approximate true diameter of 15 Å in its free state. Following the recent work of Wang *et al.*,[48] we treated the carbon atoms of the nanotube as $sp2$ carbons and used the associated atom potential functions from AMBER.[47] For the sake of simplicity in the simulations reported here, we neglected hydrodynamic interactions and implicit non-polar solvent forces in the simulations and focused on the effects of direct atom–atom interactions of the protein with nanotube atoms. We sought to determine if the

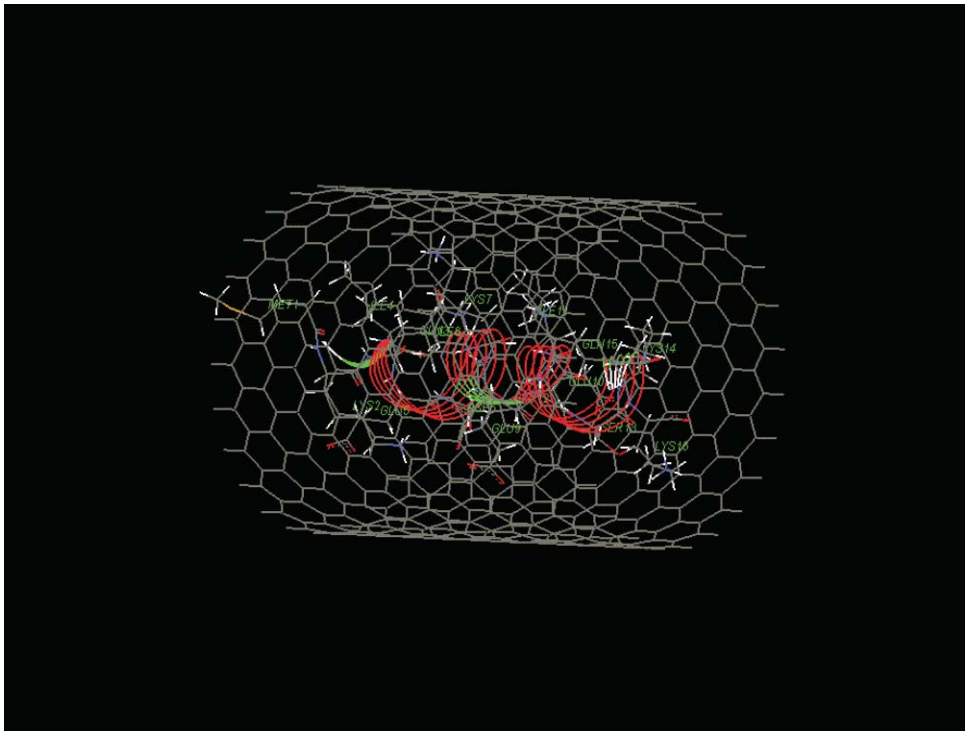

FIG. 5. $t = 0.061ns$. Helical structure maintained despite compression by nanotube.

α-helix could maintain its structure using the stiff potential constraints while moving through a rather tight fitting nanotube at a realistic transport rate. Each Brownian subunit was further treated as an isotropic particle and assigned an effective spherical radius based on its van der Waals volume and water molecular diameter. Translational and rotational diffusion coefficients were based on these effective radii.[21] A constant external axially directed force was added to the total axial component of force on each Brownian subunit of the protein in order to "thread" the protein through the nanochannel. An empirically based distance dependent dielectric function was used based on the work of Ramstein and Lavery[49] with a decay constant of 0.5Å^{-1}. Other general details of the atomistic-level BD simulation method used here can be found

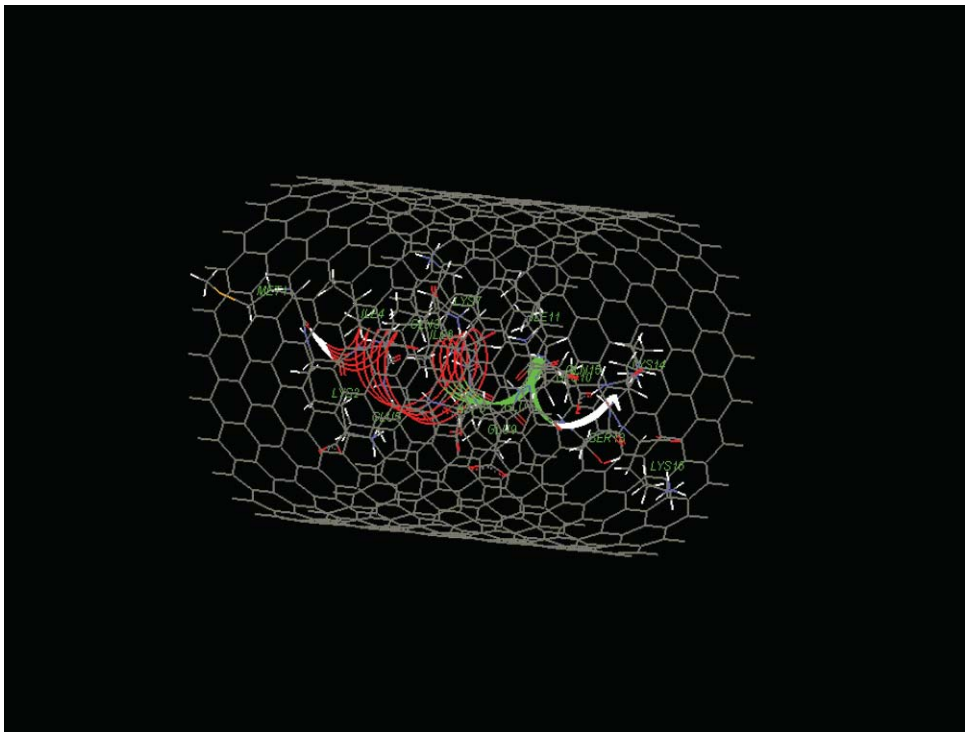

FIG. 6. $t = 0.10ns$. Screwlike motion evident.

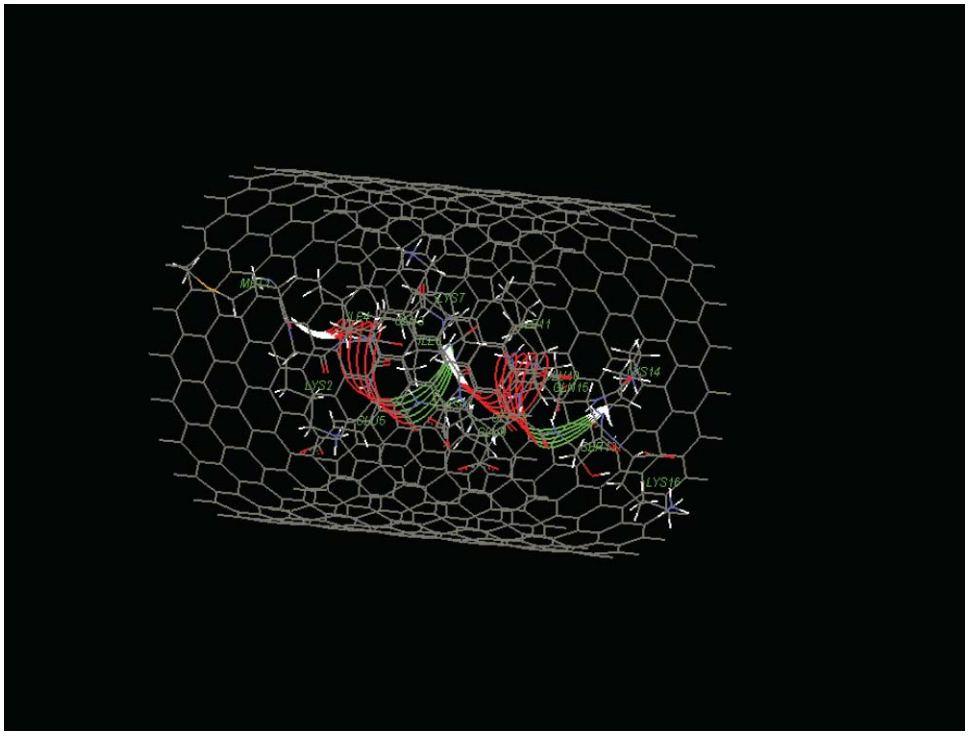

FIG. 7. $t = 0.17ns$. Three to four residues have emerged from the nanotube.

in Yang *et al.*[21] Note that all of the above assumptions could be relaxed by introducing an MD step periodically between the BD steps as outlined above.

Figures 4–7 show the real-time sequence of events as the helical protein moves through the carbon nanotube under an external driving force of 100 pN. The total real time shown is approximately 0.2 ns. The α-helix becomes slightly compressed transversely from its free configuration state as it is forced through the nanotube. The expected screwlike motion of the helix is evident from these simulations. Note that the random force was turned off in demonstrating the screw like motion shown in order to eliminate "fuzziness" in the trajectories. The stiff potential constraints employed are shown to be sufficient to maintain the integrity of the helix even under the action of the external driving force and slight compression of the helix by the nanotube. Note that a variable time step method was used[21] with a range from 50 to 100 fs. We are currently studying in detail the effects of implicit nonpolar solvent forces, hydrodynamic interactions, and dielectric behavior for these type of systems, which are beyond the scope of this study. Note that all computations shown here were conducted on a single processor SUN workstation with a total computational time less than 30 min.

VI. CONCLUSIONS

The general forms of the FP, Smoluchowski, and Langevin displacement equations, Eqs. (24), (59), (67), and (68), respectively, are the same as those obtained in the absence of external surfaces or for a single B-particle in a confined geometry. The subtle differences are associated with the specific definitions of the solvent average effects through the grand friction tensors and solvent equilibrium average force and torque acting on the B-particles. The Langevin displacement equations describing the changes in center of mass and orientations of the interacting B-particles, Eqs. (67) and (68) provide a general practical computational method for the analysis of flexible macromolecular motions in confined geometries. In general, for given initial orientations and positions of the B-particles and confining surfaces, the grand friction matrix and equilibrium average force and torque acting on the B-particles can be determined through equilibrium canonical ensemble molecular dynamics and force autocorrelation analysis.[21] In this step, the entire system is solvated and allowed to reach an equilibrium state for the solvent. The grand friction tensor, a numerical array, must be numerically inverted to obtain the grand diffusion tensor for use in Eqs. (67) and (68). The B-particles are then moved over a time step, t, to obtain their new positions and orientations. In this step, the forces, torques, and diffusion tensors are assumed approximately constant at their predetermined values according to Eqs. (67) and (68). The entire process is repeated periodically as necessary, i.e., resolvation and equilibrium MD followed by Brownian dynamics, and the B-particles' trajectories are tracked in real time. Alternatively, the implicit fluid force functions, including the friction tensors, can be approximated via *separate* analytical or computational studies for any given system, such as demonstrated in proteins.[25–27] Finally, the real-time transport of an α-helix protein through a carbon nanotube was simulated to demonstrate the ease and utility of the methods given here.

[1]X.-W. Wu and S.-S. Sung, Proteins: Struct., Funct., Genet. **34**, 295 (1999).
[2]T. Shen, C. F. Wong, and J. A. McCammon, J. Am. Chem. Soc. **123**, 9107 (2001).

[3]D. Hamelberg, T. Shen, and J. A. McCammon, J. Chem. Phys. **125**, 094905 (2006).
[4]O. F. Lange and H. Grubmuller, J. Chem. Phys. **124**, 214903 (2006).
[5]P. Szymczak and M. Cieplak, J. Chem. Phys. **127**, 155106 (2007).
[6]M. Cieplak and S. Niwieczerzal, J. Chem. Phys. **130**, 124906 (2009).
[7]T. Frembgen-Kesner and A. H. Elcock, J. Chem. Theory Comput. **5**, 242 (2009).
[8]R. M. Jendrejack, D. C. Schwartz, J. J. de Pablo, and M. D. Graham, J. Chem. Phys. **120**, 2513 (2004).
[9]J. E. Butler and E. S. G. Shaqfeh, J. Chem. Phys. **122**, 014901 (2005)
[10]C. J. Benham and S. P. Mielke, Annu. Rev. Biomed. Eng. **7**, 21 (2005).
[11]E. S. G. Shaqfeh, J. Non-Newtonian Fluid Mech. **130**, 1 (2005).
[12]J. M. Kim and P. S. Doyle, J. Chem Phys. **125**, 074906 (2006).
[13]Y. Zhang, A. Donev, T. Weisgraber, B. J. Alder, M. D. Graham, and J. J. de Pablo, J. Chem. Phys. **130**, 234902 (2009).
[14]M. Kenward and K. D. Dorfman, J. Chem. Phys. **130**, 095101 (2009).
[15]M. Muthukumar, Annu. Rev. Biophys. Biomol. Struct. **36**, 435 (2007).
[16]M. Muthukumar and C. Y. Kong, Proc. Natl. Acad. Sci. U.S.A. **103**, 5273 (2006).
[17]L. Javidpour, M. R. R. Tabar, and M. Sahimi, J. Chem. Phys. **130**, 085105 (2009).
[18]M. Zwolak and M. Di Ventra, Rev. Mod. Phys. **80**, 141 (2008).
[19]M. H. Peters, J. Chem. Phys. **110**, 528 (1999).
[20]M. H. Peters, J. Chem. Phys. **112**, 5488 (2000).
[21]Y. Zhang, M. H. Peters, and Y. Li, Proteins: Struct., Funct., Genet. **52**, 339 (2003).
[22]D. L. Ermak and J. A. McCammon, J. Chem. Phys. **69**, 1352 (1978).
[23]E. Dickinson, S. A. Allison, and J. A. McCammon, J. Chem. Soc. Faraday Trans. 2 **81**, 591 (1985).
[24]H. Abe and N. Go, Biopolymers **20**, 1013 (1981).
[25]H. J. C. Berendsen, D. van der Spoel, and R. van Drunen, Comp. Phys. Comm. **91**, 43 (1995).
[26]S. Takada, Proc. Natl. Acad. Sci. U.S.A. **96**, 11698 (1999).
[27]A. Smith and C. K. Hall, Proteins **44**, 344 (2001).
[28]D. Li, M. S. Liu, B. Ji, K. Hwang, and Y. Huang, J. Chem. Phys. **130**, 215102 (2009).
[29]A. Onufriev, D. Bashford, and D. A. Case, J. Phys. Chem. **104**, 3712 (2000).
[30]A. Onufriev and D. A. Case, J. Comput. Chem. **23**, 1297 (2002).
[31]X. Sun, T. Lin, and J. D. Gezelter, J. Chem. Phys. **128**, 234107 (2008).
[32]R. I. Cukier and J. M. Deutch, Phys. Rev. **177**, 240 (1969).
[33]G. Nienhuis, Physica **49**, 26 (1970).
[34]J. Piasecki, L. Bocquet, and J.-P. Hansen, Phys. A **218**, 125 (1997).
[35]M. Peters and R. Ying, Chem. Eng. Commun. **108**, 165 (1991).
[36]R. Mazo, J. Stat. Phys. **1**, 101 (1969).
[37]J. L. Lebowitz and Z. Rubin, Phys. Rev. **131**, 2381 (1963); P. Resbois and H. T. Davis, Physica **30**, 1077 (1964).
[38]D. W. Condiff and J. S. Dahler, J. Chem. Phys. **44**, 3988 (1966).
[39]S. Harris, J. Chem. Phys. **50**, 4820 (1969).
[40]B. Roux and T. Simonson, Biophys. Chem. **78**, 1 (1999).
[41]J. A. Wagoner and N. A. Baker, Proc. Natl. Acad. Sci. U.S.A. **103**, 8331 (2006).
[42]X.-W. Wu and S.-S. Sung, J. Comp. Chem. **19**, 1555 (1998).
[43]J.-P. Ryckaert, G. Cicotti, and H. J. C. Berendsen, J. Comp. Phys. **23**, 327 (1977).
[44]B. Hess, H. Bekker, H. J. C. Berendsen, and J. G. Fraaije, J. Comp. Chem. **18**, 1463 (1997).
[45]T. Ando, T. Meguro, and I. Yamato, Mol. Simul. **29**, 471 (2003).
[46]M. H. Peters and R. Ying, J. Chem. Phys. **98**, 6492 (1993).
[47]Y. Duan, C. Wu, S. Chowdhury, M. C. Lee, G. Xiong, W. Zhang, R. Yang, P. Cieplak, R. Luo, T. Lee, J. Caldwell, J. Wang, and P. Kollman, J. Comp. Chem. **24**, 1999 (2000).
[48]S. Wang and S. Li, Z. Cao, and T. Yan, J. Phys. Chem. C **114**, 990 (2010).
[49]J. Ramstein and R. Lavery, Proc. Natl. Acad. Sci. U.S.A. **85**, 7231 (1988).